Comput. Methods Appl. Mech. Engrg. 198 (2009) 3647–3655

Contents lists available at ScienceDirect

Comput. Methods Appl. Mech. Engrg.

journal homepage: www.elsevier.com/locate/cma

# A sampling-based approach for probabilistic design with random fields

Anirban Basudhar, Samy Missoum *

*Aerospace and Mechanical Engineering Department, The University of Arizona, Tucson, AZ, 85721, USA*

ARTICLE INFO

*Article history:*
Received 23 August 2008
Received in revised form 22 June 2009
Accepted 6 July 2009
Available online 15 July 2009

*Keywords:*
Random fields
Probabilistic design
Proper orthogonal decomposition
Support vector machine
Explicit limit state functions
Discontinuities

ABSTRACT

An original technique to incorporate random fields non-intrusively in probabilistic design is presented. The approach is based on the extraction of the main features of a random field using a limited number of experimental observations (snapshots). An approximation of the random field is obtained using proper orthogonal decomposition (POD). For a given failure criterion, an explicit limit state function (LSF) in terms of the coefficients of the POD expansion is obtained using a support vector machine (SVM). An adaptive sampling technique is used to generate samples and update the approximated LSF. The coefficients of the orthogonal decomposition are considered as random variables with distributions determined from the snapshots. Based on these distributions and the explicit LSF, the approach allows for an efficient assessment of the probabilities of failure. In addition, the construction of explicit LSF has the advantage of handling discontinuous responses. Two test-problems are used to demonstrate the proposed methodology used for the calculation of probabilities of failure. The first example involves the linear buckling of an arch structure for which the thickness is a random field. The second problem concerns the impact of a tube on a rigid wall. The planarity of the walls of the tube is considered as a random field.


## 1. Introduction

Despite substantial research efforts and recent improvements, probabilistic design still faces major challenges. First, it is well known that the initial assumptions for the representation and quantification of uncertainties are of prime importance. For instance, for a problem with spatial variability (e.g., sheet metal thickness distribution), one should choose to describe the problem with random fields as they provide a more realistic representation than uncorrelated random variables. These assumptions are as important as the process used to propagate uncertainties. Second, in a simulation-based context, the nature of the problem might severely restrict the use of traditional algorithms. Of particular interest are problems with non-smooth and discontinuous responses, prohibitive computational costs, or disjoint failure spaces. Computational design for crashworthiness is an example which encompasses these difficulties.

The probabilistic design literature is mostly dominated by approaches and applications where uncertainties are quantified as independent random variables. Techniques such as Monte Carlo simulations (MCS), and first and second order reliability methods (FORM and SORM) [1,2] are used to perform reliability assessment using assumed probability density functions (PDFs). These reliability assessment techniques are also embedded within optimization problems to carry out reliability based design optimization (RBDO) [3–5]. Many studies have also been dedicated to the reduction of computational costs associated with these reliability assessment and RBDO techniques. Approaches based on designs of experiments (DOE) and surrogate models (response surfaces and metamodels [6,7]) are common.

Recently, the authors have introduced the notion of explicit design space decomposition [8–10] whereby the LSFs are constructed explicitly in terms of the design variables. The LSF construction is based on a SVM which allows one to define the boundaries of failure regions that can be disjoint and non-convex. The approach allows for a straightforward calculation of a probability of failure using MCS. In addition, because this technique does not approximate responses but rather classify them as failed or safe, it naturally handles discontinuities. The construction of explicit LSF is also complemented by an adaptive sampling scheme which minimizes the number of function evaluations and refines the LSF approximation [10]. Therefore, the explicit design space decomposition technique is aimed at handling the difficulties due to discontinuities, complex failure domains and computational costs.

In the case of random fields, which is the focus of this article, the literature revolves around stochastic finite elements (SFE). SFE enable the propagation of uncertainties to obtain the distribution of the system's responses using polynomial chaos expansion (PCE) [11]. In order to represent a random field, it is approximated using a Karhunen–Loeve expansion [11]. The coefficients of the expansion are considered as random variables and the response

* Corresponding author.
*E-mail address:* smissoum@email.arizona.edu (S. Missoum).

0045-7825/$ - see front matter © 2009 Elsevier B.V. All rights reserved.
doi:10.1016/j.cma.2009.07.003

is expanded on a specific polynomial basis (Hermite, Legendre etc.) depending on the assumed types of probability distributions.

Several implementations of SFE are available in literature. The early approaches required the modification of the equilibrium equation to account for the uncertainty in the stiffness matrix and the load vector [11]. This approach is by construction highly intrusive and required specific codes. Newer methods developed recently overcome this limitation and allow for the determination of PCE coefficients using deterministic "black-box" function evaluations (e.g., finite element analysis). Therefore, these methods can be used with available commercial simulation packages without modifying the code [12–14].

Most studies with SFE typically assume a prior distribution of the random field. However, in practical situations, such as a random field generated by a manufacturing process, the characteristics of the random field are not known a priori. Therefore, the only way to characterize a random field with a certain level of confidence is from experimental observations. In addition, another limitation of existing approaches is that the expansion of responses on a polynomial basis hampers the use of PCE for problems with discontinuities.

In this article, an alternate non-intrusive approach is proposed, which provides a combined solution to the difficulties of realistically representing random fields, handling discontinuous responses, and efficiently calculating a probability of failure. This is achieved by combining the explicit design space decomposition approach with a proper orthogonal decomposition (POD) for the characterization of random fields.

Based on a limited number of observations, referred to as snapshots, POD is used to extract the important *features* of a random field in the form of eigenvectors of its covariance matrix [15]. The eigenvalues provide an indication of the importance of the corresponding features, thus allowing one to gauge their individual contributions to the random field. This technique is similar to the one found in pattern recognition [16].

Once the random field is characterized with the important features, the corresponding eigenvectors form a basis that is used to generate various random field configurations. This is required for design purposes as an initial set of experimental snapshots may not be sufficient. The random field is modified by varying the coefficients of the eigenvectors in the POD expansion. For this purpose, the response of the system is studied with a DOE [17,18] with respect to the coefficients of the expansion. At this stage, the actual PDFs of the coefficients are not considered, and they are assumed uniformly distributed. This is done in order to extract as much information as possible over the whole design space.

The responses, generated for each sample of the DOE, are classified into failure and non-failure using a threshold value or a clustering technique such as K-means [19]. Clustering is used in the case of discontinuous responses. These two classes are then separated in the design space using an (explicit) SVM LSF [9]. In addition, in order to refine the LSF using a limited number of samples, an adaptive sampling technique is used [10]. The sampling strategy is based on the generation of samples that maximize the probability of misclassification of the SVM while avoiding redundancy of information.

The coefficients of the POD expansion are random variables and their distributions, obtained from the snapshots, are found through basic PDF fitting techniques. A similar approach was used in [20] for the probabilistic design of turbine blade engine using POD expansion for turbine blade random geometries.

In the proposed approach, probabilities of failure are efficiently calculated using MCS. This simplicity, and this is the novelty of the proposed approach, is due to the fact that the limit state function is defined explicitly in terms of the coefficients of the POD. As mentioned previously, it is noteworthy that the accuracy of the limit state function is improved through adaptive sampling [10] to limit the number of function evaluations.

The proposed approach for the calculation of probabilities of failure is applied to two problems. The first problem consists of a three dimensional arch structure whose thickness is considered as a random field. A failure criterion is defined based on a threshold value on the critical load factor for linear buckling. The second problem involves the impact of a tube on a rigid wall. The planarity of the tube walls is modified by a random field, which leads to a global buckling (considered failure) or crushing of the tube.

## 2. Summary of the proposed approach

For the sake of clarity, this section summarizes the main steps of the approach, which are subsequently described in the following sections. The stages of the approach are (Fig. 1):

- Collection of snapshots and construction of the covariance matrix.
- Selection of the main features of the random field.
- Expansion of the field on a reduced basis. Sampling of the coefficients using a uniform design of experiments (DOE).
- Construction of an explicit LSF using SVM in the space of coefficients.
- Refinement of the LSF using adaptive sampling.
- Fitting of the probability density functions (PDF) of the POD coefficients.
- Estimation of the probability of failure using Monte-Carlo simulations (MCS).

## 3. Random field characterization

### 3.1. Data collection and covariance matrix

The first step in the characterization of a random field is the collection of several observations of the random process output (e.g., a metal sheet after forming). The process generates a scalar random field $S(\vec{X})$, function of the position $\vec{X}$. $M$ samples, outputs of this process, are obtained. On each sample, $N$ measurements are performed at distinct positions. An example of observations, referred to as snapshots, is provided in Fig. 2. The snapshots can be condensed in the following matrix:

$$\mathbf{S} = \begin{pmatrix} S_{11} & \cdots & S_{1M} \\ \vdots & \ddots & \vdots \\ S_{N1} & \cdots & S_{NM} \end{pmatrix} \tag{1}$$

The general term $S_{ij}$ is the $i$th measurement on the $j$th snapshot. A matrix $\mathbf{\Phi}$ is then defined, whose general term is:

$$\Phi_{ij} = S_{ij} - \overline{S_i}, \tag{2}$$

where $\overline{S}$ is the average snapshot vector given by

$$\overline{S_i} = \frac{1}{M}\sum_{j=1}^{M} S_{ij} \tag{3}$$

The covariance matrix $\mathbf{C}$, which is a square matrix of size $N$, is obtained as:

$$\mathbf{C} = \frac{1}{M}\mathbf{\Phi}\mathbf{\Phi}^T \tag{4}$$

Since the number of measurement locations $N$ is usually high, the covariance matrix is large.

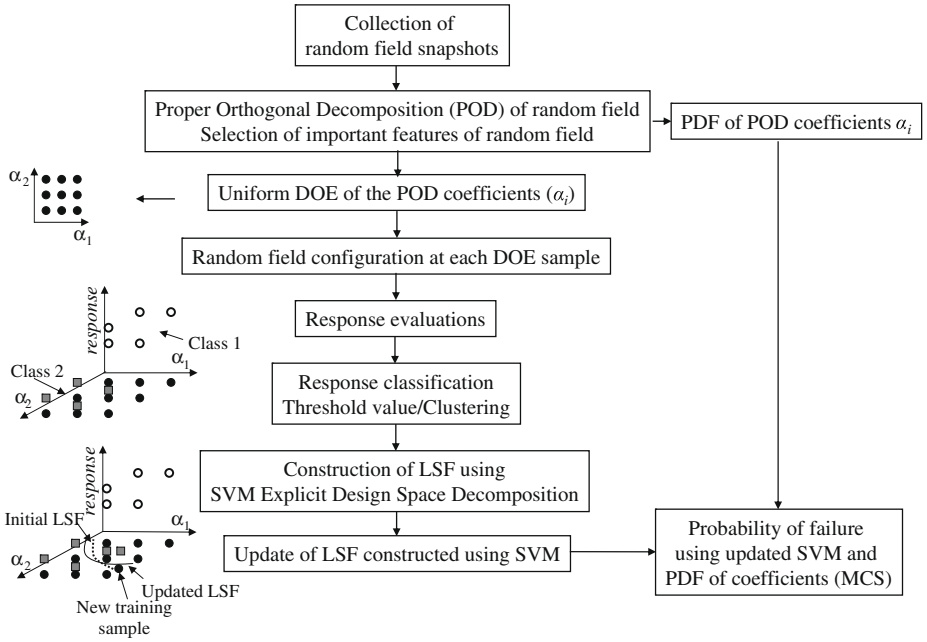


**Fig. 1.** Summary of the proposed methodology.

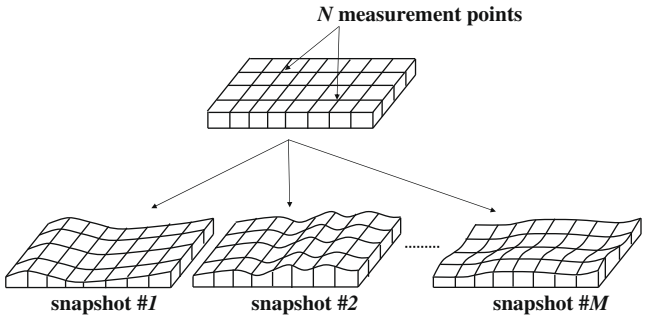


**Fig. 2.** Example of $M$ snapshots with $N$ measurement points.

### 3.2. Feature extraction and selection – POD

Proper orthogonal decomposition (POD) is used to decompose the random field on a basis made of the eigenvectors of the covariance matrix [21].

The random field is expressed in terms of the eigenvectors (i.e. features) as:

$$S_i = \overline{S} + \sum_{j=1}^{j=M} \alpha_{ij} V_j \tag{5}$$

$S_i$ is the measurement vector of the $i$th snapshot. $V_j$ is the $j$th eigenvector of the covariance matrix and $\alpha_{ij}$ are coefficients. The eigenvectors being orthogonal, the general expression of the coefficients is obtained by projection:

$$\alpha_{ij} = \frac{\Phi_i . V_j}{\|V_j\|^2}, \tag{6}$$

where $\Phi_i = S_i - \overline{S}$ is the $i$th centered snapshot and $\|.\|$ is the Euclidean norm. For normalized eigenvectors $\|V_j\| = 1$, and the coefficients are:

$$\alpha_{ij} = \Phi_i \cdot V_j \tag{7}$$

If the size of covariance matrix is large then finding the eigenvectors might be difficult. If the number of snapshots $M$ is lower than $N$, the eigenvectors can be obtained efficiently by defining a matrix $\mathbf{C}'$ as:

$$\mathbf{C}' = \frac{1}{M} \mathbf{\Phi}^T \mathbf{\Phi} \tag{8}$$

The eigenvectors of the covariance matrix $\mathbf{C}$ can then be found as [22,16]:

$$V_i = \mathbf{\Phi} V_i', \tag{9}$$

where $V_i'$ is an eigenvector of $\mathbf{C}'$. The dimensionality of the square matrix $\mathbf{C}'$ being $M$, the solution of the eigenvalue problem is computationally more efficient.

Once the eigenvectors of the covariance matrix are obtained, the "important" features are selected by investigating the relative magnitude of the corresponding eigenvalues. The magnitude of an eigenvalue is proportionally related to the importance of the corresponding feature. Therefore by ranking the $M$ eigenvalues, the $MS$ most important features can be selected. This ranking is typically performed by inspecting the ratio $\rho_i$ of the $i$th eigenvalue to the sum of all eigenvalues [23]:

$$\rho_i = \frac{\lambda_i}{\sum_{j=1}^{M} \lambda_j} \tag{10}$$

The final expression of the expansion reads:

$$\widetilde{\Phi_i} = \sum_{j=1}^{j=MS} \alpha_{ij} V_j, \tag{11}$$

where $\widetilde{\Phi_i}$ is the approximate reconstruction of the $i$th centered snapshot. The expansion containing less than $M$ eigenvectors can only approximately reconstruct the original snapshots. The mean square error due to the truncation of the expansion is given by the following relation [11]:

$$\epsilon^2 = \frac{1}{M} \sum_{j=1}^{j=M} \left( S_j - \widetilde{S_j} \right)^2 = \sum_{j=MS+1}^{M} \lambda_j \tag{12}$$

The upper bound of the sum is $M$ and not $N$, since all the eigenvalues from $M+1$ to $N$ are zero ($\mathbf{C}'$ and $\mathbf{C}$ have the same eigenvalue fractions).

### 3.3. Probability density functions of the POD expansion coefficients

In order to perform probabilistic design, the PDFs of the coefficients need to be identified using data from the $M$ snapshots. The coefficients are calculated for each snapshot using Eq. (6). Thus, a distribution consisting of $M$ discrete values is obtained for each of the $MS$ coefficients. It is then possible to fit Weibull or Beta distributions to the data (Fig. 8) that will be used subsequently for the calculation of the probability of failure.

## 4. Sampling-based coefficient selection and response estimation

The characterization of a random field, and coefficient distributions is accomplished using the data from the snapshots. However, the mere characterization of the random field is not sufficient to account for uncertainties in the design process. For this purpose, several instances of random fields (other than the snapshots) are created by using different linear combinations of the eigenvectors.

The combinations are defined by selecting the POD coefficients using a DOE. The bounds of the DOE are defined by the maximum and minimum values of the coefficients obtained based on the snapshots. At this stage, the coefficients are sampled uniformly, and their PDFs are not yet taken into account. This is done to obtain information uniformly over the entire coefficient space. The DOE used for this study is generated by Latinized Centroidal Voronoi Tessellations (LCVT) [18], as it provides a uniform distribution in the space. An example of an LCVT DOE is shown in Fig. 3.

The system response is estimated at each sample using a simulation code, such as a finite element software. The responses obtained for the DOE samples are then classified into failure or safe categories, based on a threshold response value or by using a clustering method such as K-means (Fig. 4). The classification of responses into two distinct classes provides the information needed to generate the explicit LSF as explained in the following section.

## 5. Explicit limit state function construction using SVM

### 5.1. Explicit limit state function

SVM is a classification tool that belongs to the class of machine learning techniques. The main feature of SVM lies in its ability to explicitly define complex decision functions that optimally separate two classes of data samples. Thus, once the coefficient samples are categorized into two classes, SVM can provide an explicit decision function (the limit state function) separating the distinct classes. The equation of the SVM LSF is given by equating the quantity $s$ in Eq. (13) equal to zero [24].

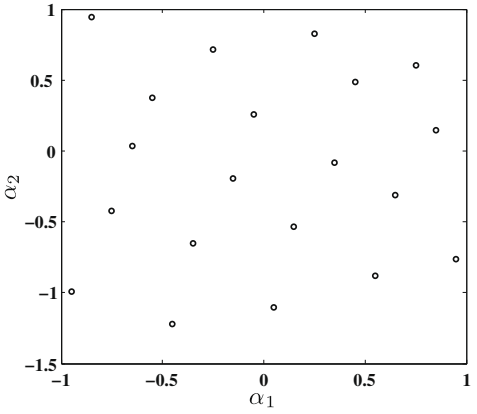


**Fig. 3.** Example of LCVT DOE using 20 samples.

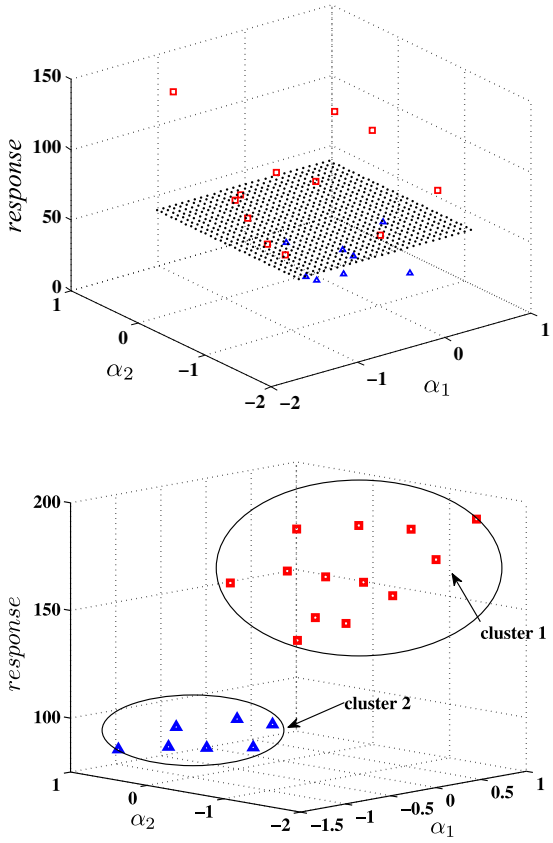


**Fig. 4.** Classification of response values using a threshold value (top) and clustering (bottom).

$$s = b + \sum_{i=1}^{NSV} \lambda_i y_i K(\mathbf{x}_i, \mathbf{x}), \tag{13}$$

where $\mathbf{x_i}$ is a vector in the space, $K$ is a kernel function, $y_i$ is the class label corresponding to $\mathbf{x_i}$ that can take values $\pm 1$, and $b$ is the bias. $NSV$ is the number of support vectors, which are the samples lying on $s = \pm 1$. Several kernel functions can be used, like polynomial, Gaussian radial basis function, or splines [24]. The Gaussian kernel is used for this study. An example of explicit LSF construction using SVM is shown in Fig. 5.

The construction of an explicitly defined LSF allows one to associate different regions of the space with distinct system behavior. It

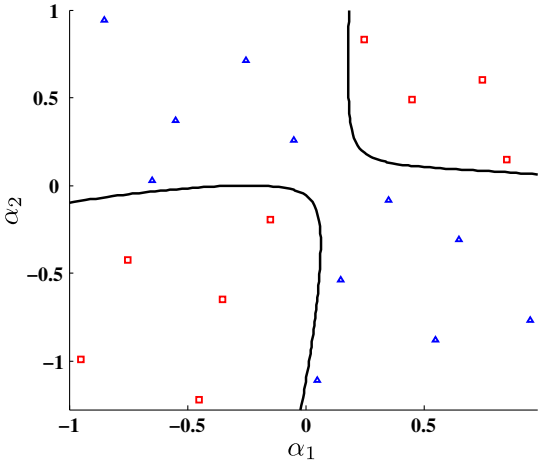


**Fig. 5.** Example of an explicit SVM LSF.

is then easy to calculate the probability of failure using the explicitly defined LSF, as predicting the class of a sample involves the calculation of an analytical function.

### 5.2. Adaptive sampling

In order to predict the explicit LSF with a reduced number of samples, an adaptive sampling technique [10,25] is used to select the coefficients. The sample size of the initial LCVT DOE is kept small, and a first approximation of the LSF is made. Subsequent samples are then selected on the previous SVM decision function (LSF), as the probability of misclassification is highest on the decision function. This leads to an efficient update of the SVM LSF.

The stopping criterion for the SVM update algorithm is based on quantifying the change in the LSF between two successive iterations. A set of $N_{conv}$ convergence points are defined for this purpose, and the change is quantified as the fraction of convergence points changing their class (i.e. sign of SVM) between iterations $k$ and $k+1$:

$$\Delta_k = \frac{num(|sign(s^i_{k-1}) - sign(s^i_k)| > 0)}{N_{conv}} \tag{14}$$

In order to implement a practical stopping criterion, the fraction $\Delta_k$ is then fitted by an exponential curve:

$$\hat{\Delta}_k = Ae^{Bk}, \tag{15}$$

where $\hat{\Delta}_k$ represents the fitted values of $\Delta_k$. $A$ and $B$ are the parameters of the exponential curve. For the update to stop, the value of the fitted $\hat{\Delta}_k$ and its slope at the last iteration, should simultaneously be less than small positive numbers $\epsilon_1$ and $\epsilon_2$, respectively.

## 6. Probability of failure calculation – MCS

The explicit LSF allows one to efficiently calculate the probability of failure using MCS. The PDFs of the coefficients, as found in Section 3.3, are used to generate Monte-Carlo samples. Predicting failure or non-failure at these samples involves calculating the sign of the analytical expression of the LSF (Eq. (13)). An example of calculation of the probability of failure is depicted in Fig. 6.

## 7. Examples

### 7.1. Linear buckling of an arch structure

This section provides an example of the effect of a random field on the critical load factor of an arch structure. The structure is subjected to a unit pressure load on the top surface. The thickness of the arch should ideally be constant over the entire surface; however it may vary due to uncertainties in the manufacturing processes. These variations are represented, for this study, by an artificial analytical random field (as opposed to real experimental data). The arch has a radius of $R$ = 200 mm, and it subtends an angle of $\theta_{max} = 60^\circ$ at the center (Fig. 7). The width of the arch is $w$ = 600 mm, and in the absence of any uncertainty it has a thickness $t$ = 3 mm. The random field representing the deviation from the mean thickness is assumed to have the following form.

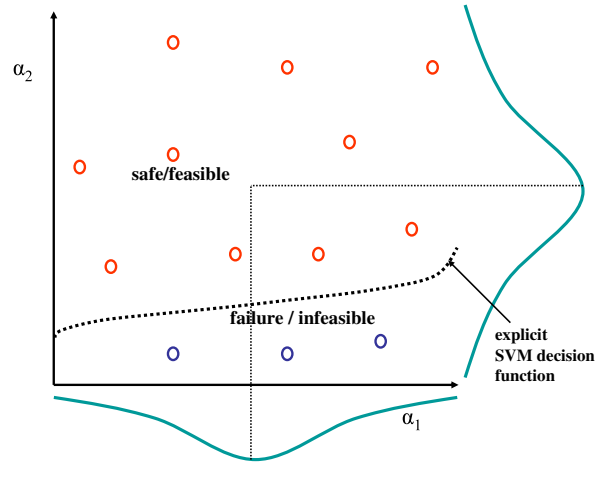


**Fig. 6.** Probability of failure calculation using MCS.

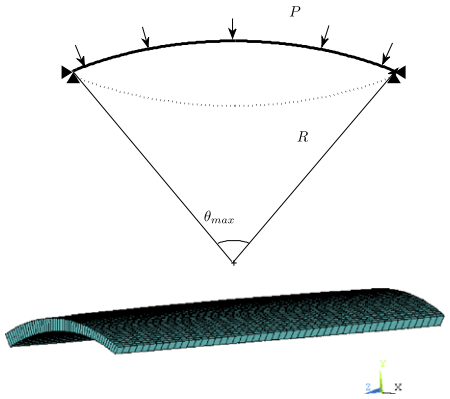


**Fig. 7.** Geometry and loading of the arch structure. The bottom figure shows the variation of thickness in space for one snapshot.

$$h(\theta, z) = \frac{1}{4}\cos\left(\frac{K\Pi\theta}{\theta_{max}}\right)\sin\left(\frac{L\Pi z}{w}\right) \tag{16}$$

The snapshots are created by randomly selecting values of $K$ and $L$. $K$ and $L$ are uniformly distributed in an interval ranging from 0.7 to 1.3.

Following the creation of the snapshots, the important features are extracted based on the corresponding eigenvalue fractions. For example, if 200 snapshots are created, the four first ratios of eigenvalues as defined in Eq. (10) are 0.7208, 0.1325, 0.0800, and 0.0634. The remaining ratios are clearly very small, and can be considered equal to zero. The analysis of the system is done by approximating the random field with three features.

Without the change in thickness introduced due to the random field, the critical load factor is 2.3086. When variations due to the random field are included, the critical load of the structure may increase or decrease. To quantify the uncertainty, the probability of having a critical load factor greater than 90% of the deterministic critical load factor is calculated. A critical load factor less than 90% of the deterministic critical load factor is considered as failure.

#### 7.1.1. Random field approximation with three features

The first three features are used to approximate the random field. The corresponding eigenvalue fractions add up to 0.933. The random field is described as:

$$S(\alpha_1, \alpha_2, \alpha_3) = \alpha_1 V_1 + \alpha_2 V_2 + \alpha_3 V_3, \tag{17}$$

where $\alpha_1, \alpha_2$, and $\alpha_3$ are the coefficients of the expansion. The minimum and maximum values of the coefficients, obtained from the snapshots, are given in Table 1. The PDFs of the coefficients are shown in Fig. 8. Coefficients $\alpha_1$ and $\alpha_2$ are fitted to Beta distributions, while a Weibull distribution is used to fit $\alpha_3$.

Once the random field is characterized, the coefficients $\alpha_1, \alpha_2$, and $\alpha_3$ are sampled uniformly using 40 initial LCVT samples. The random fields corresponding to these configurations of the coefficients are reconstructed using Eq. (17). The critical load factor for each configuration is then obtained using a finite element analysis (using ANSYS). The samples are then classified using the aforementioned

**Table 1**
Arch Problem. Ranges of coefficients based on the snapshots.

| Coefficient | Minimum value | Maximum value |
|---|---|---|
| $\alpha_1$ | −7.1718 | 5.2072 |
| $\alpha_2$ | −3.6051 | 3.2182 |
| $\alpha_3$ | −3.2041 | 3.2232 |

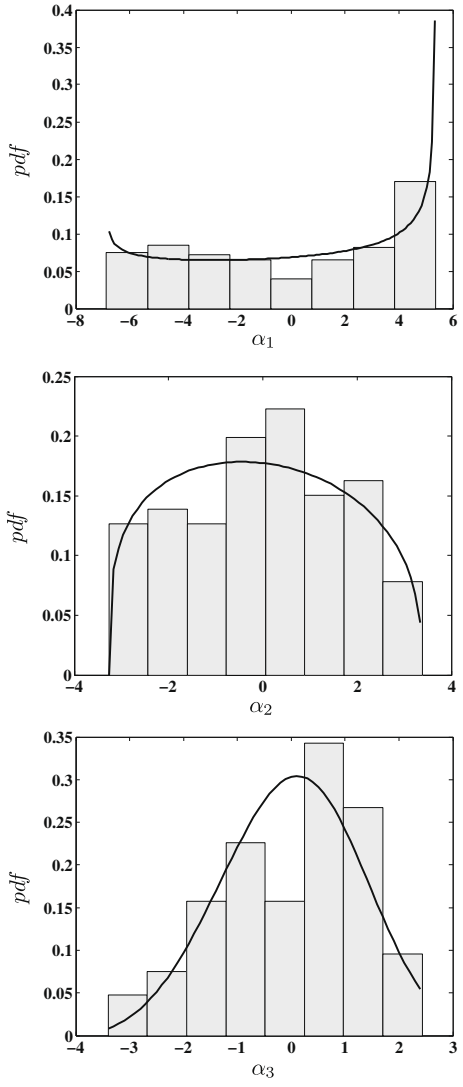


**Fig. 8.** PDF for coefficients $\alpha_1$, $\alpha_2$, and $\alpha_3$ corresponding to the first three features for the arch problem.

failure criteria, and the classified configurations are the training samples for SVM to predict an initial LSF. It is then refined using the update algorithm, to construct the final LSF with 79 samples (Fig. 9). The convergence of the SVM update algorithm is shown in Fig. 10.

After obtaining the explicit LSF, MCS is carried out to calculate the probability of failure using the PDFs the coefficients (Fig. 8). In order to validate the predicted value of $P_f$, MCS is carried out with 10,000 samples while varying the values of $K$ and $L$ with their assumed distributions. Finite element analysis are carried out at each of these samples to find the actual probability of failure. The results are collected in Table 2.

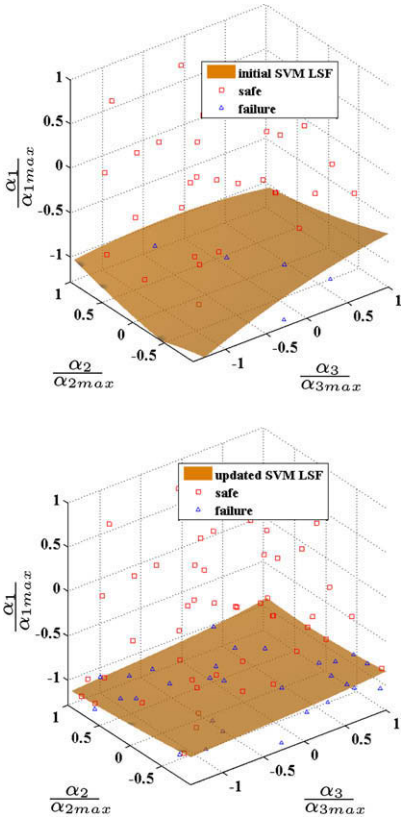


**Fig. 9.** Initial (top) and final (bottom) SVM LSF for the arch problem with three features. The brown surface is the LSF separating failure (blue triangles) and safe (red squares) classes. (For interpretation of the references to colour in this figure legend, the reader is referred to the web version of this article.)

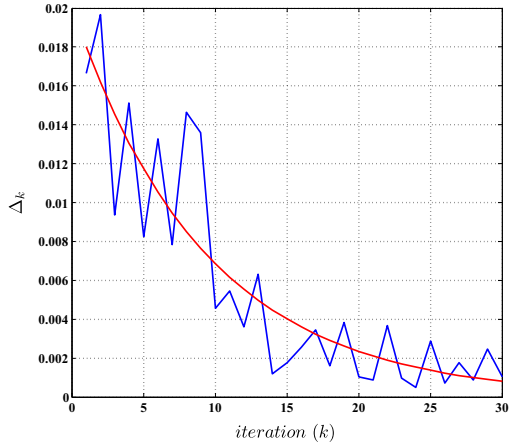


**Fig. 10.** Convergence of the SVM LSF update for the arch problem.

*7.1.2. Study of the influence of number of snapshots*

In order to select the number of snapshots $M$, its influence on the eigenvalue fractions $\rho_i$ are studied for the arch problem (Fig. 11). It is seen that there is a significant change in the values of $\rho_i$ initially. The values gradually stabilize around a constant value. A constant value suggests that adding snapshots does not provide much information to the random field. It is observed that the amplitude of the perturbations decreases gradually, and a value of $M = 200$ is selected.

**Table 2**
Arch Problem. Comparison of predicted and actual probabilities of failure.

| | SVM-based MCS | Brute-force MCS |
|---|---|---|
| Monte-Carlo samples | $10^6$ | $10^4$ |
| $P_f$ | 0.1291 | 0.1418 |
| 95% confidence interval | [0.1284, 0.1298] | [0.1350, 0.1487] |

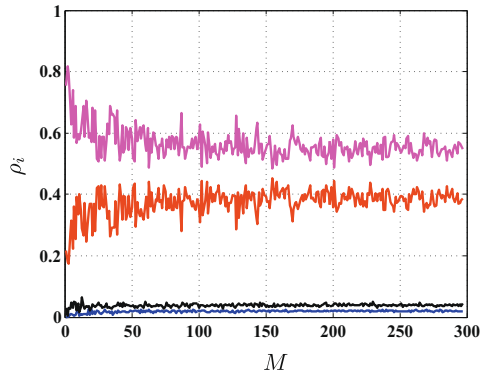


**Fig. 11.** Influence of the number of snapshots ($M$), shown for the first four features of the arch problem. $\rho_i$ ($i$=1,2,3,4) are the eigenvalue fractions corresponding to the first four features.

### 7.2. Tube impacting a rigid wall

In this section the application of the proposed methodology is shown on an impact problem. A tube of length $l = 1$ m (Fig. 12) is made to impact a rigid wall with velocity 15 m/s, and the resulting behavior is analyzed. The cross-section of the tube is a square with side $a = 7$ cm, and four masses of 25 kg each are attached to the four rear corners. The two bottom corners in the front of the tube are constrained in the transverse directions. The planarity of the walls of the tube are modified by a random field given by:

$$h(x_L, z_L) = \frac{A}{1000}\cos\left(\frac{3\Pi x_L}{a}\right)\sin\left(\frac{L\Pi z_L}{l}\right), \tag{18}$$

where $x_L$ and $z_L$ are the local coordinates at the four faces. $x_L$ varies between $-\frac{a}{2}$ and $+\frac{a}{2}$, while $z_L$ takes values between 0 and $-l$. $A$ and $L$ are uniformly distributed random variables with ranges $[0.25, 0.75]$ m and $[1, 2]$, respectively. The parameter $A$ modifies the amplitude of the random field, while the frequency is modified by $L$. 200 snapshots of the random field are created, by varying $A$ and $L$. The important features are then extracted using POD. The first three ratios (Eq. (10)) of eigenvalues are 0.6985, 0.2630, and 0.0383. Only the first two features are selected to characterize the random field.

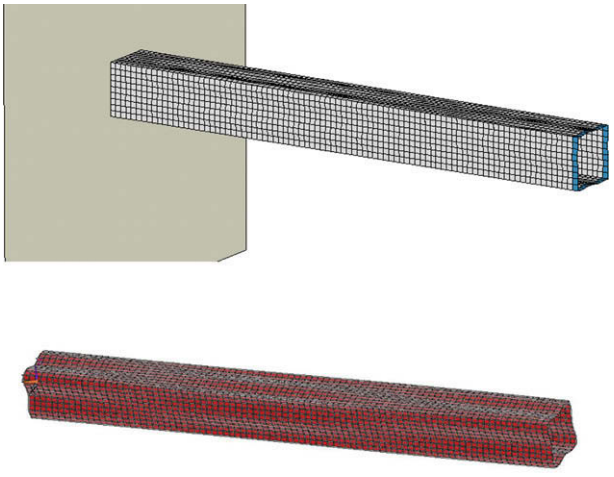

**Fig. 12.** Tube impacting rigid wall. The bottom figure shows the effect of the random field.

The impact behavior of the tube falls into two main categories-crushing and global buckling (Fig. 13). Due to the effect of the ran-

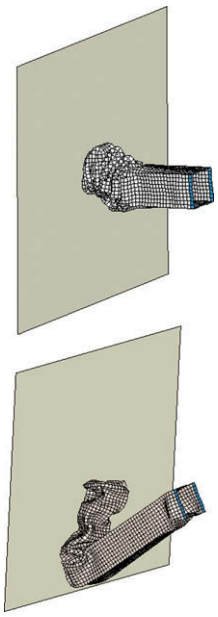

**Fig. 13.** Crushing (top) and global buckling (bottom) of a tube subjected to impact.

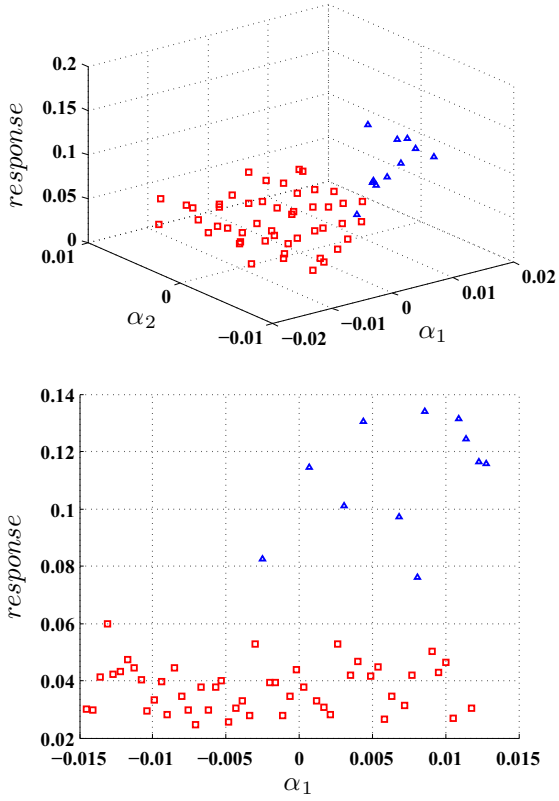


**Fig. 14.** Discontinuous behavior of the tube response with respect to the coefficients of the expansion. The bottom figure shows a two-dimensional view of the top figure.

dom field, the behavior can undergo sudden change from one state to the other. The discontinuous behavior of the tube is shown in Fig. 14.

It is desired that the tube should display crushing, and there should not be any global buckling. In order to quantify the behavior, the maximum of the two absolute transverse displacements in $x$ and $y$ directions is studied. A low value of this quantity indicates crushing behavior, while a large value shows that global buckling has occurred. The probability of failure (global buckling), due to the effect of the random field, is studied with a thickness of 1.5 mm. The method can also be extended to carry out optimization by including the design variables as additional dimensions to the space (e.g., length or thickness).

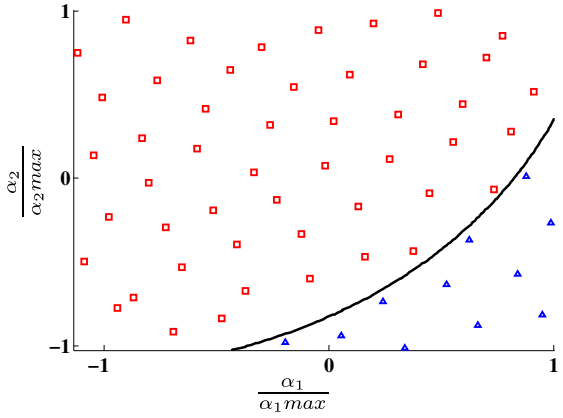


**Fig. 15.** SVM LSF with two features. The black curve is the LSF separating global buckling (blue triangles) and crushing (red squares). (For interpretation of the references to colour in this figure legend, the reader is referred to the web version of this article.)

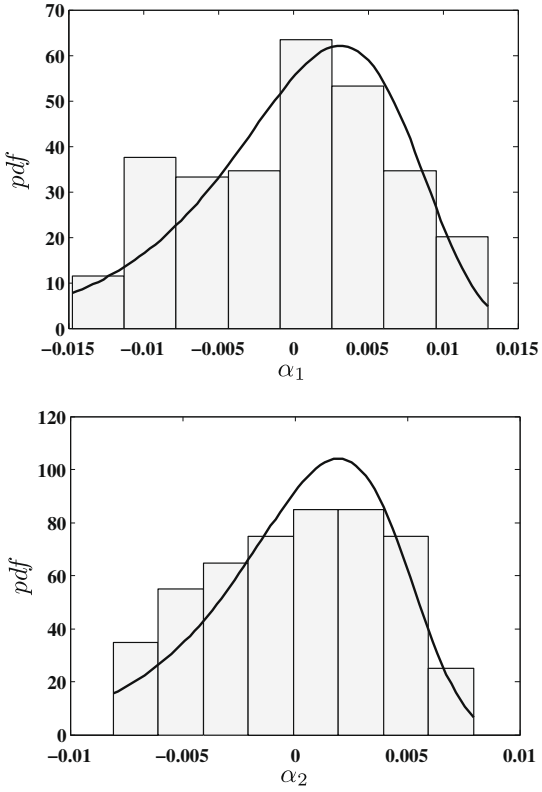


**Fig. 16.** PDF for coefficients $\alpha_1$, and $\alpha_2$ corresponding to the first two features for the tube problem.

Following the random field characterization, the coefficients $\alpha_1$, and $\alpha_2$ are sampled uniformly using 60 LCVT samples, and the corresponding random field instances are constructed using Eq. (11). The ranges of the two coefficients are $[-0.0148, 0.0130]$ and $[-0.0081, 0.0079]$. The analysis is done using ANSYS LS-DYNA, to find the transverse displacements. The samples are then classified using K-means clustering, and the classified configurations are used as training samples for SVM to predict the explicit LSF (Fig. 15). After obtaining the explicit LSF, the probability of failure is calculated using the PDFs of the coefficients shown in Fig. 16. The coefficient $\alpha_1$ is fitted using a Weibull distribution, while $\alpha_2$ is fitted with a Beta distribution. $10^6$ MCS samples are used, and $P_f$ is found as 0.1243.

## 8. Conclusion

A technique for reliability assessment using random fields is proposed. A new sampling-based method is used for constructing various potential random field configurations. The method overcomes the need for assumption on the random field distribution by using experimental data and Proper Orthogonal Decomposition. In addition the SVM-based method of constructing explicit LSFs enables one to address discontinuous system responses, which is successfully shown in the case of the tube impact problem. In future study, the method will be extended for carrying out probabilistic optimization. This can be easily performed by adding the design variables as additional dimensions of the space while constructing the decision function. In the present study, analytical random fields have been used due to lack of experimental data; in the future, the methodology will be applied to data obtained from actual experiments.

## Acknowledgement

The support of the National Science Foundation (Award CMMI-0800117) is gratefully acknowledged.

## References

[1] A. Haldar, S. Mahadevan, Probability, Reliability, and Statistical Methods in Engineering Design, Wiley and Sons, New York, 2000.
[2] R. Melchers, Structural Reliability Analysis and Prediction, John Wiley & Sons, 1999.
[3] G. Kharmanda, A. Mohamed, M. Lemaire, Efficient reliability-based design optimization using a hybrid space with application to finite element analysis, Struct. Multidiscip. Opt. 24 (2002) 233–245.
[4] B.D. Youn, K.K. Choi, Selecting probabilistic approaches for reliability-based design optimization, AIAA J. 42 (1) (2004) 124–131.
[5] B.A. Adams, M.S. Eldred, J.W. Wittwer, Reliability-based design optimization for shape design of compliant micro-electro-mechanical systems, in: 11th Symposium AIAA/ISSMO on Multidisciplinary Analysis and Optimization, Portsmouth, Virginia, September 2006.
[6] D. Huang, T.T. Allen, W.I. Notz, R.A. Miller, Sequential kriging optimization using multiple-fidelity evaluations, Struct. Multidiscip. Opt. 32 (2006) 369–382.
[7] B.J. Bichon, M.S. Eldred, L.P. Swiler, S. Mahadevan, J.M. McFarland, Multimodal reliability assessment for complex engineering applications using efficient global optimization, in: Proceedings of the 48th conference AIAA/ASME/ASCE/AHS/ASC on Structures, Dynamics and Materials, Paper AIAA-2007-1946, Honolulu, Hawaii, April 2007.
[8] S. Missoum, P. Ramu, R.T. Haftka, A convex hull approach for the reliability-based design of nonlinear transient dynamic problems, Comput. Meth. Appl. Mech. Engrg. 196 (2007) 2895–2906.
[9] A. Basudhar, S. Missoum, A.H. Sanchez, Limit state function identification using support vector machines for discontinuous responses and disjoint failure domains, Prob. Engrg. Mech. 23 (1) (2008) 1–11.
[10] A. Basudhar, S. Missoum, Adaptive explicit decision functions for probabilistic design and optimization using support vector machines, Comput. Struct. 86 (19–20) (2008) 1904–1917.
[11] R. Ghanem, P.D. Spanos, Stochastic Finite Elements: A Spectral Approach, Springer, 1991.
[12] D. Ghiocel, R. Ghanem, Stochastic finite element analysis of seismic soil structure interaction, J. Engrg. Mech. ASCE 128 (1) (2002) 66–77.

[13] M. Berveiller, B. Sudret, M. Lemaire, Non linear non intrusive stochastic finite element method – application to a fracture mechanics problem, in: Ninth International Conference on Structural Safety and Reliability (ICOSSAR'2005), Rome, Italy, 2005.
[14] S. Huang, S. Mahadevan, R. Rebba, Collocation-based stochastic finite element analysis for random field problems, Prob. Engrg. Mech. 22 (2007) 194–205.
[15] S. Missoum, Probabilistic optimal design in the presence of random fields, Struct. Multidiscip. Opt. 35 (6) (2008) 523–530.
[16] M. Turk, A. Pentland, Eigenfaces for recognition, J. Cogn. Neurosci. 3 (1) (1991) 71–86.
[17] D.C. Montgomery, Design and Analysis of Experiments, Wiley and Sons, 2005.
[18] Vincente J. Romero, John V. Burkardt, Max D. Gunzburger, Janet S. Peterson, Comparison of pure and "latinized" centroidal Voronoi tesselation against various other statistical sampling methods, J. Reliab. Engrg. Syst. Safety 91 (10–11) (2006).
[19] J.A. Hartigan, M.A. Wong, A k-means clustering algorithm, Appl. Stat. 28 (1979) 100–108.
[20] T. Bui-Thanh, Model-constrained optimization methods for reduction of parameterized large-scale systems, PhD thesis, MIT, Cambridge, MA, June 2007.
[21] Y.C. Liang, H.P. Lee, S.P. Lim, W.Z. Lin, K.H. Lee, C.G. Wu, Proper orthogonal decomposition and its applications – Part I: Theory, J. Sound Vibr. 252 (3) (2002) 527–544.
[22] L. Sirovich, Turbulence and the dynamics of coherent structures – Part 1: Coherent structures, Quart. Appl. Math. 45 (3) (1987) 561–571.
[23] T. Bui-Thanh, M. Damodaran, K. Willcox, Proper orthogonal decomposition extensions for parametric applications in transonic aerodynamics, in: 21st AIAA Applied Aerodynamics Conference, Orlando Florida, Orlando, Florida, September 2003.
[24] S.R. Gunn, Support vector machines for classification and regression, Technical Report ISIS-1-98, Department of Electronics and Computer Science, University of Southampton, 1998.
[25] A. Basudhar, S. Missoum, Parallel update of failure domain boundaries constructed using support vector machines, in: Seventh World Congress on Structural and Multidisciplinary Optimization, Seoul, Korea, May 2007.